

See discussions, stats, and author profiles for this publication at: <https://www.researchgate.net/publication/273298595>

# Interplay of Substrate Surface Energy and Nanoparticle Concentration in Suppressing Polymer Thin Film Dewetting

ARTICLE in MACROMOLECULES · JANUARY 2015

Impact Factor: 5.8 · DOI: 10.1021/ma501262x

---

CITATIONS

6

---

READS

37

## 4 AUTHORS, INCLUDING:



Sudeshna Roy

IIT Kharagpur

7 PUBLICATIONS 45 CITATIONS

[SEE PROFILE](#)



Alamgir Karim

University of Akron

307 PUBLICATIONS 6,937 CITATIONS

[SEE PROFILE](#)



Rabibrata Mukherjee

IIT Kharagpur

35 PUBLICATIONS 422 CITATIONS

[SEE PROFILE](#)

## Interplay of Substrate Surface Energy and Nanoparticle Concentration in Suppressing Polymer Thin Film Dewetting

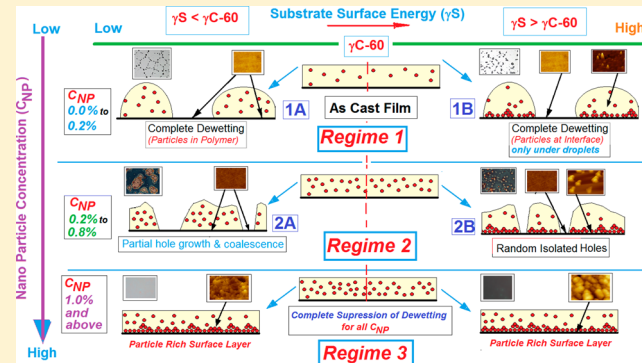
Sudeshna Roy,<sup>†,‡</sup> Diya Bandyopadhyay,<sup>‡</sup> Alamgir Karim,<sup>\*,‡,§</sup> and Rabibrata Mukherjee<sup>\*,†</sup>

<sup>†</sup>Instability and Soft Patterning Laboratory, Department of Chemical Engineering, IIT Kharagpur, Kharagpur, West Bengal 721302, India

<sup>‡</sup>Department of Polymer Engineering and <sup>§</sup>Akron Functional Materials Centre (AFMC), University of Akron, Akron, Ohio 44325, United States

### Supporting Information

**ABSTRACT:** It is known that dewetting of a polystyrene (PS) thin film on a silicon substrate gets completely suppressed upon addition of small amount of  $C_{60}$  nanoparticles (NP).<sup>1</sup> The NPs migrate to the film–substrate interface and forms an enriched surface layer of the particles that eventually stabilizes the film by apparent pinning. In this article we quantitatively highlight the unexplored effect of substrate surface energy ( $\gamma_s$ ) on the migration of the NPs to the film–substrate interface and their contribution on dewetting suppression. Depending on the relative magnitudes of NP concentration ( $C_{NP}$ ) and  $\gamma_s$ , we identify three distinct stability regimes. In regime 1 ( $C_{NP} < 0.2\%$ ) there is no suppression of dewetting and the final polygonal arrangement of droplets closely resemble dewetted structures in particle free films. However, the size of the polygons becomes smaller in NP containing films when  $\gamma_s < \gamma_{C60}$  (NP surface energy) and larger as  $\gamma_s$  exceeds  $\gamma_{C60}$ . In regime 2 ( $0.3\% < C_{NP} < 0.75\%$ ) the films dewet partially, and the extent of dewetting is seen to strongly dependent on the relative magnitudes of  $\gamma_{C60}$  and  $\gamma_s$ . While dewetting proceeds up to the stage of partial hole growth and coalescence when  $\gamma_s < \gamma_{C60}$ , some random isolated holes are seen to form when  $\gamma_s > \gamma_{C60}$ . On the basis of direct AFM imaging, we show that in both regimes 1 and 2 the NPs migrate to the substrate–film interface only when  $\gamma_s > \gamma_{C60}$ . We show complete suppression of dewetting in regime 3 ( $C_{NP} > 1.0\%$ ), where the particles are seen to migrate to the substrate for all values of  $\gamma_s$ . The work highlights that entropy driven migration of particles takes place on substrates with any  $\gamma_s$  only above a critical NP concentration ( $C_{NPC}$ ) and only on substrates with  $\gamma_s > \gamma_{C60}$  when  $C_{NP} < C_{NPC}$ . The findings, apart from dewetting suppressing, can guide potential design criteria for applications such as electron extracting layer in organic photovoltaic.



### INTRODUCTION

Thin polymer films coated on solid surfaces find extensive applications ranging from organic photovoltaic to coatings, adhesives, biological membranes, sensors, nonlinear optical devices, and so on. Though such films are easy to create by simple solution processing techniques such as dip or spin coating,<sup>2</sup> their long-term stability is an important issue that is yet to be fully resolved.<sup>3–15</sup> Films thinner than ~100 nm spontaneously become unstable and rupture, particularly on nonwettable substrates, due to competing thermodynamic and kinetic factors, such as attractive interfacial van der Waals forces (spinodal dewetting),<sup>3</sup> variation in density of the polymer with film thickness,<sup>4</sup> sudden release of residual stresses accumulated during film preparation, etc.<sup>5</sup> Slightly thicker films dewet due to nucleation of holes.<sup>6,9</sup> Most often, thin polymer films rupture and dewet the solid substrate, with the formation and growth of holes.<sup>7</sup> Typically, a distinct rim appears around each growing hole due to mismatch in the rates at which polymer is dislodged from the substrate surface and is redistributed to the intact

parts of the film by diffusion and flow.<sup>7,8</sup> With time, the rims of adjacent growing holes merge with each other and form narrow polymer threads, which subsequently break up into isolated droplets due to Rayleigh instability.<sup>7,8</sup> The morphological evolution sequence, mechanism, and various other aspects of polymer thin film instability and dewetting, including the role of viscoelasticity and slippage, has been extensively investigated over the past few years.<sup>9–15</sup> Though dewetting is gaining acceptance as a viable mesopatterning technique, particularly in conjugation with suitable templating strategies,<sup>12–15</sup> the phenomenon is undesirable from the standpoint of coating application, and therefore, stabilization of ultrathin films against rupture is important both fundamentally and from the standpoint of coating applications.

Received: June 18, 2014

Revised: December 23, 2014

Several strategies have been adopted to stabilize ultrathin films and make them resistant against spontaneous rupture and dewetting.<sup>16–41</sup> The earliest approach was to graft compatibility enhancing polymer chains at the film-substrate interface to modify the wettability of the substrate and make the films stable.<sup>16,17</sup> Other approaches include chemical modification of the polymer by *in situ* photochemical cross-linking with photoactive molecules such as bis(benzophenol),<sup>18</sup> incorporation of high molecular weight end-functionalized chains for enhancing specific affinity toward the substrate,<sup>19</sup> inter- and intramolecular ionomer complexation by sulfonation,<sup>20</sup> etc. These approaches are however difficult to implement under practical conditions and at large scales, as most of them involve either modifying the substrate or film properties.

A simple, generic approach which has become popular for suppressing dewetting is addition of nanofillers to the polymer films in extremely small quantities.<sup>1,21–41</sup> This was first demonstrated by Barnes et al., who could stabilize 20–50 nm thick, spinodally unstable PS and polybutadiene (PB) thin films on nonwettable substrates by adding fullerene ( $C_{60}$ ) nanoparticles in extremely low quantities (0.1–5% w/w). Depending on  $C_{NP}$ , dewetting was either partially ( $C_{NP} < 1\%$ ) or completely suppressed ( $C_{NP} \geq 1\%$ ).<sup>1,21–25</sup> Following this approach, thin films of several polymers could be stabilized by adding additives,<sup>21–25</sup> such as nanoparticles (NP) of silica,<sup>26</sup> carbon black,<sup>26</sup> CdSe quantum dots,<sup>27,28</sup> gold NP,<sup>29,30</sup> polystyrene,<sup>27,31</sup> polybenzyl ether dendrimers,<sup>32</sup> polyhedral oligomeric silsesquioxane (POSS) and cyclopentyl-substituted POSS (CpPOSS),<sup>33–35</sup> star-branched nanogel (NG) molecules comprising a cross-linked divinylbenzene (DVB) core with poly(methyl methacrylate) (PMMA) arms,<sup>36</sup> TMPC (tetramethylbisphenol A polycarbonate),<sup>37</sup> complex perovskite [ $(C_6H_5C_2H_4NH_3)_2PbI_4$ ] molecules,<sup>38</sup> star comb-like four-arm polymer molecules of P(S-*ran*-VB-g-PMMA),<sup>39</sup> single- and multiwalled carbon nanotubes (CNT),<sup>40,41</sup> etc. Apart from dewetting inhibition, controlling nanoparticle dispersion in a polymer matrix is a problem of significant importance and is the key to achieve dramatic property enhancement in polymer nanocomposites.<sup>42,43</sup>

Based on detailed scrutiny of published literature, it is observed that only in few cases the particles/molecules remain within the polymer matrix and suppression of dewetting is attributed to rheological modification of the film in the presence of the particles.<sup>29,30,39–41</sup> However, in the majority of the cases the particles migrate to the film–substrate interface and form a diffused immobilized interfacial layer, which screens the polymer–substrate interaction, imparts pinning to the contact line, and suppresses dewetting. The formation of the interfacial particle layer was first interpreted from neutron reflectivity measurements<sup>1</sup> and later directly visualized using an atomic force microscope (AFM) in fullerene-containing films.<sup>23</sup> The particle migration is attributed to an entropy driven mechanism known as depletion attraction and is mostly observed in bare inorganic nanoparticles which are not compatible to the organic polymer chains.<sup>44</sup> In simple terms, during annealing the polymer chains in the film expel a fraction of the particles toward the substrate, a process that allows the polymer chains to gain conformational entropy, as they do not have to stretch around the particles in the film.<sup>42</sup> Krishnan et al. have shown that the loss in the translational entropy as well as the enthalpy of mixing of the particles is offset by the gain in the conformational entropy of the linear polymer chains, as they are dislodged from the substrate due to the migrating

particles.<sup>45–47</sup> At higher  $C_{NP}$ , complete coverage by the enriched layer effectively modifies the wetting properties of the substrate and stabilizes the films.<sup>1,21,26–28</sup> Even at lower  $C_{NP}$ , when the enriched layer fails to cover the entire substrate, it still arrests the growth of the ruptured holes by pinning the contact line, resulting in partially dewetted films.<sup>1,21,26–28,39</sup> In a recent paper, Cabral and co-workers argued that photoinduced oxidation and cross-linking of the  $C_{60}$  NPs might also be responsible for suppression of dewetting.<sup>47</sup> It must be highlighted that nanoparticles grafted with polymer molecules do not migrate to the substrate–film interface and exhibit an opposite tendency, as these “hairy” nanoparticles behave as amphiphiles and migrate to the free surface (film-air interface) due to the unfavorable interaction between the nonpolar organic grafts and the polar core of the inorganic NPs.<sup>48–50</sup> Maillard et al. have shown that such grafted particles, depending on the graft density, might self-organize at the free surface when the shielding effect is poor (sparse grafting) or simply fill and jam the surface without any structure formation if the grafting density is adequate to prevent particles from attaching to each other.<sup>49</sup> Recently, Basu and co-workers have shown that the tendency of migration of the grafted NPs reduce with enhanced confinement (reduced film thickness), which favors dispersion of the particles.<sup>50</sup>

A key aspect related to NP-induced suppression of dewetting that has not been systematically studied is how  $\gamma_S$  and the relative magnitudes of the interfacial energies between the different components ( $\gamma_{S-C_{60}}$ ,  $\gamma_{S-PS}$  and  $\gamma_{C_{60}-PS}$ ) influence the migration of the particles, formation of the immobilized interfacial layer, and finally suppression of dewetting. The original study by Barnes et al. was performed on silicon oxide surfaces having relatively high value of  $\gamma_S \approx 70$  mJ/m<sup>2</sup>. Only recently, Cabral and co-workers briefly reported some experimental observation of the influence of  $\gamma_S$  on the dewetting/suppression of dewetting of  $C_{60}$  NP containing thin PS films.<sup>47</sup> A detailed study on the combined influence of  $\gamma_S$  and  $C_{NP}$  on dewetting suppression is reported in this article, based on studying thermal dewetting of 112 nm thick PS films containing fullerene NPs with different  $C_{NP}$ , on substrates with different  $\gamma_S$  varying between ~28 and 59 mJ/m<sup>2</sup>. The film thickness ( $h$ ) has been kept constant at 112 nm in all the experiments reported in this article. A recent paper describes how addition of  $C_{60}$  NPs to a 112 nm thick film of a PS and PB blends accelerates the rate of dewetting, but with morphological variations, when annealed in the bulk single-phase versus two-phase regimes.<sup>51,52</sup> Thus, a choice of  $h = 112$  nm allows direct comparison between the influence of  $C_{60}$  NP addition on the stability and dynamics of a homopolymer film to that of a phase separating/nonphase separating polymer blend thin film with the same thickness.<sup>51,52</sup> We do understand that the value of  $h$  will certainly influence the stability of the system. However, the system is already complex with several parameters and varying  $h$  will make the data more complicated and difficult to interpret. Thus, the effect of  $h$  on stability of thin films on substrates with different  $\gamma_S$  is not included here and will be taken up separately. Additionally, a 112 nm thick PS film is spinodally stable, as the long-range destabilizing interfacial van der Waals interaction becomes weak when  $h \geq 100$  nm,<sup>6,9</sup> and therefore films in this thickness range do find practical applications in membranes, polymer field effect transistors, resist layer in lithography, etc.<sup>15</sup> Such films are however prone to nucleated rupture and therefore ensuring the stability films in this thickness range on different  $\gamma_S$  substrates is important for various applications.<sup>6,9,12</sup>

## MATERIALS AND METHODS

Monodispersed polystyrene (PS) with average molecular weight  $M_w = 3000$  g/mol and polydispersity index (PDI) of 1.09 (Polymer Source Inc.) was used in our experiments. The choice of the  $M_w$  is such that it matches previous NP induced dewetting studies and therefore allows direct comparison.<sup>1</sup> Laboratory grade toluene was used as the solvent for dissolving PS, the concentration of which in the final solution was maintained at 3% (w/w). The solution was stirred overnight and screened through a 0.20  $\mu\text{m}$  PTFE microfilter before adding the  $C_{60}$  NPs (purity >99%, Sigma-Aldrich), which were dispersed in toluene separately and ultrasonicated inside a nitrogen-purged glovebox, before adding it to the filtered PS solution. A series of PS solution with same dilution (3%) but with different NP concentration, varying between 0 and 3.0% (wt of particle/wt of polymer), were prepared. The NP containing polymer solutions were sonicated for 30 min prior to spin coating.

The 20 mm  $\times$  20 mm square pieces of cleaned p-type Si (100) wafers (Silicon Quest International, USA) with 1.5 nm thick native oxide layer were used as substrates. Different  $\gamma_s$  substrates were created by first silanizing the wafers and then exposing the silanized wafers to UV ozone (UVO) irradiation for different durations.<sup>53,54</sup> Prior to silanization, the wafers were blown with a nitrogen jet to remove any dust particle and exposed to UVO for 15 min in a UVO chamber (Novascan, USA, Model: PSD Pro UV-4) to remove any organics and oxide buildup. For silanization, the cleaned wafers were immersed in a dilute solution of octyltriethoxysilane (OTES) in a mixture of *n*-hexadecane and chloroform for 24 h, which results in the formation of a self-assembled monolayer (SAM) of the silane molecules on the substrate surface. The silanized wafers were first rinsed with chloroform followed by DI water and finally dried in dry  $N_2$ . Silanization of the silicon wafer substrates with OTES results in a surface with relatively low  $\gamma_s \approx 28.04$  mJ/m<sup>2</sup>. To generate substrates with different  $\gamma_s$ , the silanized wafers were exposed to UVO for different durations. UV irradiation at 184.9 nm wavelength dissociates molecular oxygen into atomic oxygen. The atomic oxygen combines with the molecular oxygen to produce ozone, which subsequently gets dissociated by the 253.7 nm UV irradiation.<sup>53,54</sup> The OTES molecules absorb the short wavelength UV radiation and react with the atomic oxygen available in close proximity of the surface, resulting in oxidation of the surface chemical moieties. The extent of surface oxidation depends on the amount of atomic oxygen available, which is proportional to the time of UV exposure ( $t_E$ ). Consequently,  $\gamma_s$  of the substrates progressively increases with longer  $t_E$ .<sup>48</sup> The  $\gamma_s$  of the substrates were measured using contact angle goniometry (Ramé Hart) using standard probing liquids, the details of which are available in section 1.0 of the Supporting Information. Substrates with the following  $\gamma_s$  were used in our experiments: 28.08 mJ/m<sup>2</sup> (no UV exposure), 31.05 mJ/m<sup>2</sup> ( $t_E = 2$  min), 38.35 mJ/m<sup>2</sup> ( $t_E = 4$  min), 42.31 mJ/m<sup>2</sup> ( $t_E = 6$  min), 46.53 mJ/m<sup>2</sup> ( $t_E = 8$  min), 50.88 mJ/m<sup>2</sup> ( $t_E = 10$  min), 52.87 mJ/m<sup>2</sup> ( $t_E = 12$  min), 54.28 mJ/m<sup>2</sup> ( $t_E = 15$  min), 56.23 mJ/m<sup>2</sup> ( $t_E = 17$  min), 58.50 mJ/m<sup>2</sup> ( $t_E = 20$  min), and 58.50 mJ/m<sup>2</sup> ( $t_E = 30$  min).

The NP containing PS films were spin-coated (Laurel Technologies, USA, and Apex Instruments, India) on the substrates immediately after the UVO exposure to eliminate possible surface contamination. The film thickness ( $h = 112 \pm 3$  nm) was measured using an ellipsometer (EP3, Accuron GmBH, Germany). After spin coating, the films were annealed at 60 °C for 1 h to remove any remnant solvent. To engender dewetting, the films were annealed at 130 °C for 46 h inside a vacuum oven, after which the final morphologies were examined using an optical microscope (Leica DM2500). Some samples were annealed for more than 46 h, but no subsequent morphological evolution was observed.

Some intact as well as dewetted films were peeled off from the substrates in order to examine the film–substrate interface and investigate possible formation of the immobilized particle layer. As the AFM cantilever tip diameter is of the order of 15 nm, it is not possible to identify a single NP but a cluster of NPs or a layer (enhanced RMS roughness in comparison to a bare silicon substrate) could be easily

identified and imaged following this approach. For performing these experiments, the films (as cast as well as after annealing) were peeled off from the substrate using a sticky cross-linked PDMS (Sylgard 184, Dow Corning USA) block following protocol described elsewhere.<sup>23</sup> The Sylgard 184 block was prepared at a ratio of 20:1 of base to curing agent and thermally annealed at 120 °C for 12 h. Once fully cross-linked, the block was brought in conformal contact with the film and was subsequently immersed in water.<sup>54</sup> Water wets at the interface between the silicon wafer and the PS film and facilitates transfer of the film to the PDMS block. In a slight modification to the previously reported protocol,<sup>23</sup> we used a heated Sylgard block (heated at about 80 °C) which ensured better adhesion of the film to the block facilitating easy peel off. Once the film was removed, the enriched particle layer or clusters on the substrate was directly imaged using an AFM (PicoScan S100, Agilent Technologies, USA).

## RESULTS AND DISCUSSION

We calculated the interfacial energy between the particle and the polymer ( $\gamma_{C_{60}-PS}$ ), between the polymer and the substrate ( $\gamma_{PS-Sub}$ ), and between the substrate and the particles ( $\gamma_{Sub-C_{60}}$ ) as a function of  $\gamma_s$ , which is schematically shown in Figure 1. The

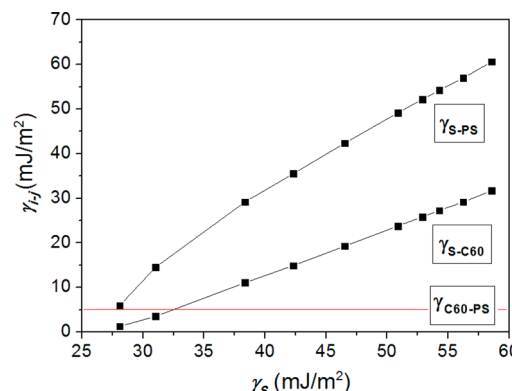
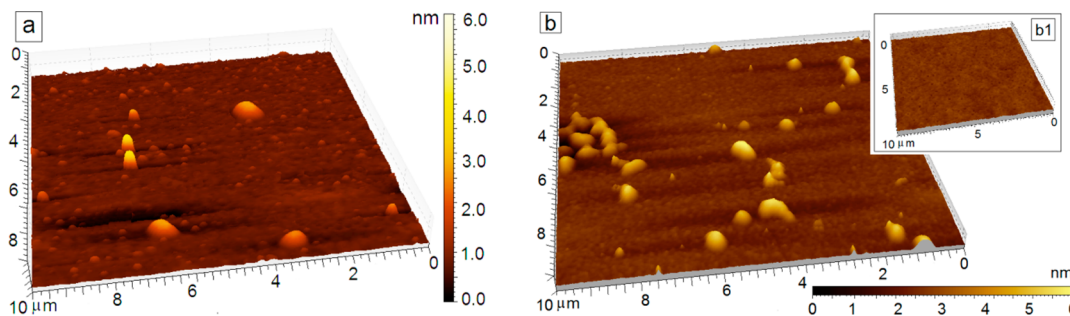


Figure 1. Variation of  $\gamma_{s-PS}$  and  $\gamma_{s-C_{60}}$  with  $\gamma_s$ . The value of  $\gamma_{C_{60}-PS}$  is also indicated on the plot.

equation and the procedure used for calculation are mentioned in the Supporting Information (section 1.0). The value of  $\gamma_{PS-C_{60}}$ , which does not change with  $\gamma_s$ , is also shown in the figure. From Figure 1, it can be seen that both  $\gamma_{s-C_{60}}$  and  $\gamma_{s-PS}$  increase with increase in  $\gamma_s$ . However,  $\gamma_{s-PS}$  increases at a much higher rate than  $\gamma_{s-C_{60}}$ . This can be attributed to completely apolar nature of PS and enhanced polarity of the substrate with increase in  $\gamma_s$  (refer to Table S2, Supporting Information). As a consequence, a high  $\gamma_s$  substrate prefers to remain covered with a layer of weakly polar  $C_{60}$  particles than completely apolar PS. We define a new term,  $E_p = \gamma_{s-PS} - \gamma_{s-C_{60}}$  which is an indicator of the energy penalty associated with a substrate being covered with PS and being covered by an immobilized layer of particles. A higher positive value of  $E_p$  implies preferred migration of the particles toward the interface, which is seen to increase with increase in  $\gamma_s$ . Same is the trend in variation of the free energy of adhesion [ $\Delta G_{C_{60}-PS-s} = \gamma_{s-C_{60}} - (\gamma_{s-PS} + \gamma_{C_{60}-PS})$ ] with  $\gamma_s$ , which is shown in Table S3 of the Supporting Information. However, a consideration based only on EP or  $\Delta G_{C_{60}-PS-s}$  is far from being complete as neither of them considers the entropic effects, which is strongly associated with long-chain polymer molecules in the presence of the nanoparticles.

The as-cast NP containing films are smooth and appear to be featureless under an optical microscope, for all  $C_{NP}-\gamma_s$



**Figure 2.** Particle clusters seen on the substrate surface after peeling off as-cast films having  $C_{NP} = 1.0\%$  on (a) low ( $\gamma_s = 28.04 \text{ mJ/m}^2$ ) and (b) high ( $\gamma_s = 58.50 \text{ mJ/m}^2$ ) surface energy substrates. Inset b1 shows the scan of the PDMS block to which the peeled film is attached, which is featureless, indicating that the particles remain immobilized onto the substrate surface during peeling.

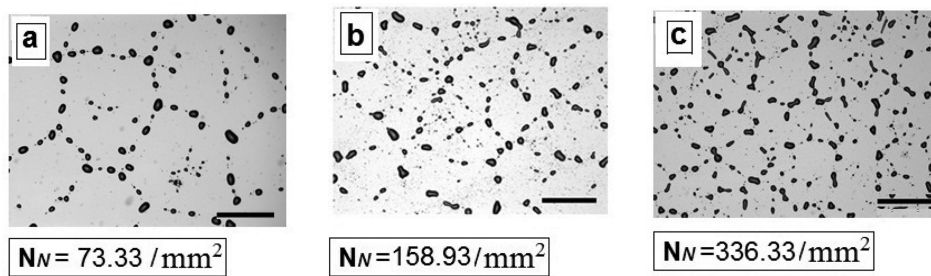


**Figure 3.** Optical microscopy images of completely dewetted 112 nm thick particle free films, annealed for 46 h at 130 °C. The surface energy ( $\text{mJ/m}^2$ ) of the substrate is (a) 28.04, (b) 42.31, and (c) 58.50  $\text{mJ/m}^2$ . Scale bar = 100  $\mu\text{m}$ .

combinations (shown in Figure S2 of the Supporting Information). The AFM scan of the films surfaces confirms that the films are smooth with an RMS roughness  $<1 \text{ nm}$  (insets of Figure S2e,f, Supporting Information), confirming that during spin coating no particles migrate to the film–air interface irrespective of  $C_{NP}$  and  $\gamma_s$ , the reason for which has already been discussed in the Introduction. Figure 2 shows the AFM scans of the film–substrate interfaces for films with  $C_{NP} \geq 1.0\%$ , where we observe the formation of tiny particle clusters right after spin coating on substrates having  $\gamma_s = 28.04 \text{ mJ/m}^2$  (Figure 2a) and  $\gamma_s = 58.50 \text{ mJ/m}^2$  (Figure 2b), respectively. Similar interfacial particle clusters, right after spin coating were also observed in films with  $C_{NP} = 2.0\%$ , on substrates with any  $\gamma_s$  (Figure S3c, Supporting Information). Comparison between Figures 2a and 2b reveals that the number density of particle clusters increases with increase in  $\gamma_s$  ( $0.07 \pm 0.02/\mu\text{m}^2$  in Figure 2a;  $0.26 \pm 0.03/\mu\text{m}^2$  in Figure 2b), though the average dimension of each cluster remains nearly the same ( $235.4 \pm 31.2 \text{ nm}$ ). Though the AFM tip cannot individually identify a particle, as the tip radius of curvature ( $\approx 15 \text{ nm}$ ) is much larger than the particles diameter ( $\approx 3 \text{ nm}$ ), yet the clusters observed in both figures correspond to a maximum of 2–3 particle layers, as their height ( $\approx 6 \text{ nm}$ ) is roughly twice the particle diameter. A complementary scan of the peeled film attached to the Sylgard block shows a nearly flat morphology (inset to Figure 2b). The question to ask at this point is whether some particle (clusters) also transfers along with the PS film during the peeling stage. The phase image of the peeled films however did not reveal any additional contrast, thereby allowing us to conclude that the particle clusters do not get dislodged from the substrate during the peeling process. Also, we did not observe any shallow craters on the surface of the peeled PS film, which one might expect corresponding to the interfacial particle clusters. We feel that the low molecular weight of the PS film flattens these craters by flow, particularly as a heated Sylgard

block is used for peeling. Peeled films attached to the Sylgard blocks were identically featureless for other  $\gamma_s$ – $C_{NP}$  combinations as well. The mechanism for the migration of the particles to the film–substrate interface during spin coating in higher  $C_{NP}$  films is discussed later.

**Complete Dewetting of Particle Free Films (Control Experiments).** To contrast the stability and dynamics of the NP containing films with the particle free ones, we first examine the morphology of particle free dewetted PS films on different  $\gamma_s$  substrates. The three frames of Figure 3 shows the dewetted morphology of a particle free film on substrates with  $\gamma_s = 28.04$ , 42.31, and 58.50  $\text{mJ/m}^2$ , respectively. The morphology of the dewetted films on substrates with other  $\gamma_s$  can be seen in Figure S4 of the Supporting Information. Upon thermal annealing for 46 h, the particle free films dewetted completely forming droplets arranged along polygons (Figure 3), irrespective of  $\gamma_s$ . The final morphology in all the cases bears a clear signature of nucleated dewetting of the films by the formation of random, isotropic holes, followed by their growth, coalescence of adjacent rims, formation of cellular shaped polymer threads, and finally breakup of the threads into isolated droplets due to Rayleigh instability.<sup>6–9</sup> The size of the polygons (obtained by analyzing Figure 3 and Figure S4) becomes progressively smaller with gradual increase in  $\gamma_s$ . This in turn leads to progressive increase in the number density of polygons ( $N_N$ ). The variation of  $N_N$  with  $\gamma_s$  is plotted in Figure 4 (symbol ■), which shows that  $N_N$  increases linearly with  $\gamma_s$  at a rate of  $7.693 \text{ mJ}^{-1} \text{ mm}^{-2}$ . The observation implies that with increase in  $\gamma_s$ , more number of holes appears during the dewetting process. Once a film has ruptured due to nucleation of a hole, the driving force for hole growth is determined by the imbalance of surface and interfacial tensions acting along the contact line. It can be understood from Young's equation that the driving force reduces with an increase in  $\gamma_s$ . Thus, the dewetting dynamics is fastest on the lowest  $\gamma_s$  substrate (Figure 3a) and progressively

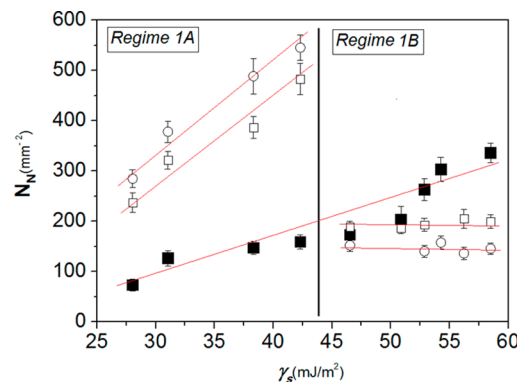


**Figure 4.** Variation of number density of the features with surface energy of the substrate. (■) Particle free film; (□) film with  $C_{NP} = 0.1\%$ ; (○) film with  $C_{NP} = 0.2\%$ . The lines indicate best fit to the data, the slopes of which are  $7.693 \pm 0.229 \text{ mJ}^{-1} \text{ mm}^{-2}$  (particle free);  $14.861 \pm 2.099 \text{ mJ}^{-1} \text{ mm}^{-2}$  ( $C_{NP} = 0.1\%$ ) and  $16.894 \pm 2.045 \text{ mJ}^{-1} \text{ mm}^{-2}$  ( $C_{NP} = 0.2\%$ ). For the particle containing films the fit has been done only for regime 1A. Regime 1B for both the particle containing films gives a slope  $\approx 0$ .

slows down with gradual increase in  $\gamma_s$ , due to reduced driving force.<sup>56</sup> A slower dynamics of the film allows more time for more number of holes to nucleate over the intact parts of the film on higher  $\gamma_s$  substrates. Appearance of larger number of holes limits the maximum size of each hole as the adjacent rims starts merging with each other. This leads to the formation of more number of polygons with thinner and narrower threads, eventually leading to increase in  $N_N$  with increasing  $\gamma_s$ .

**Complete Dewetting of Films with Low NP Concentration ( $C_{NP} < 0.2\%$ ).** The three frames of Figure 5 show the dewetted morphology of a film with  $C_{NP} = 0.1\%$  on substrates with  $\gamma_s = 28.04, 42.31$ , and  $58.50 \text{ mJ/m}^2$ , respectively. The dewetted morphology of the films on substrates with other  $\gamma_s$  for  $C_{NP} = 0.1\%$  and  $C_{NP} = 0.2\%$  can be seen in Figures S5 and

S6 of the Supporting Information. It can be seen that the films dewet completely irrespective of the  $\gamma_s$  forming droplets aligned along polygons in both cases. The calculated values of  $N_N$  when plotted as a function of  $\gamma_s$  show that the trend of  $N_N$  increasing monotonically with  $\gamma_s$  in particle free films gets altered in particle-containing films. In films with both  $C_{NP} = 0.1\%$  and  $0.2\%$ , the polygon size progressively reduce ( $N_N$  increases) as long as  $\gamma_s \leq 42.31 \text{ mJ/m}^2$ , which we mark as regime 1A in Figure 4. For  $\gamma_s \geq 46.53 \text{ mJ/m}^2$ ,  $N_N$  becomes nearly independent of  $\gamma_s$ , which is identified as regime 1B. It is further seen that in regime 1A the magnitude of  $N_N$  in NP containing films is higher than that of particle free films, and on a substrate of specific  $\gamma_s$ ,  $N_N$  increases with increase in  $C_{NP}$ . In contrast, in regime 1B,  $N_N$  in particle-containing films is lower than  $N_N$  in particle free films on a substrate with identical  $\gamma_s$  and also  $N_N$  reduces with increase in  $C_{NP}$ . The qualitative reasoning for these observations is discussed later. Notably, the transition between regimes 1A and 1B occurs around a critical magnitude of  $\gamma_s \approx 43 \text{ mJ/m}^2$ , which is close to the surface energies of both the particles ( $\gamma_{C60} = 41.7 \text{ mJ/m}^2$ ) and that of the polymer ( $\gamma_{PS} = 42.1 \text{ mJ/m}^2$ ). Thus, it apparently becomes difficult to immediately conclude if the transition takes place as  $\gamma_s$  exceeds  $\gamma_{PS}$  or  $\gamma_{C60}$ . The issue however be resolved with the help of Figure 4, which shows that there is no change in the trend of variation in  $N_N$  around  $\gamma_s \approx 43 \text{ mJ/m}^2$  in particle free films, and therefore it is logical to conclude that the regime crossover is attributed to the presence of the particles and depends on the relative magnitudes of  $\gamma_{C60}$  and  $\gamma_s$  and not on the magnitude of  $\gamma_s$ .

In order to gain deeper insight on the precise role of the  $C_{60}$  NPs on dewetting of low  $C_{NP}$  films in each regime, we investigated the substrate–film interface with an AFM, after peeling the dewetted droplets. The interface is featureless for a film with  $C_{NP} = 0.1\%$  on a substrate with  $\gamma_s = 28.04 \text{ mJ/m}^2$  (Figure S7, Supporting Information). AFM scanning at different areas reveal that the interface is featureless and flat

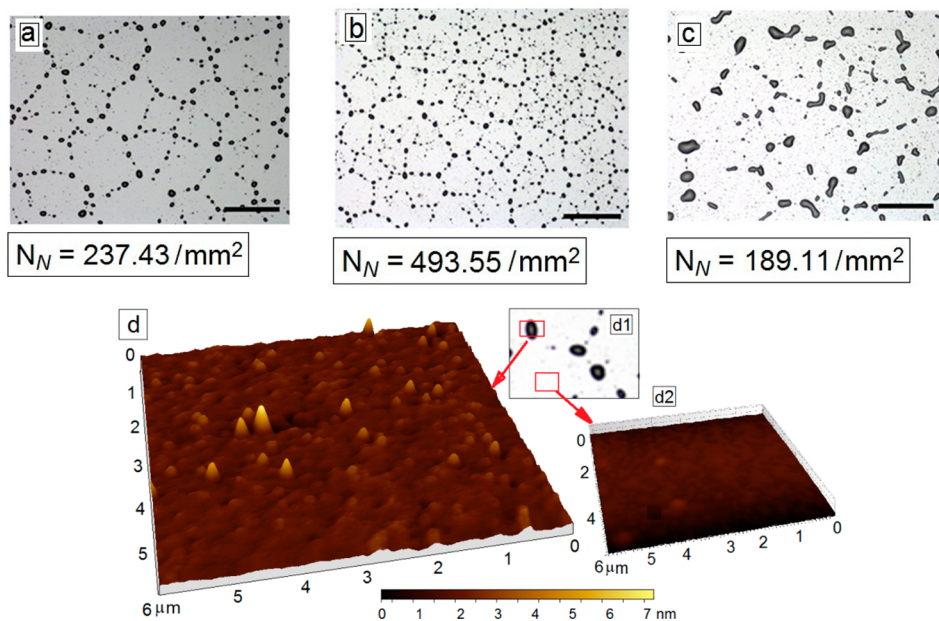


**Figure 5.** (a–c) Optical microscopy images of completely dewetted 112 nm thick films with  $C_{NP} = 0.1\%$  on substrates with  $\gamma_s$  = (a) 28.04, (b) 42.31, and (c) 58.50  $\text{mJ/m}^2$ . Scale bar n all the frames = 100  $\mu\text{m}$ . (d) Isolated particle clusters are seen on a high surface energy substrate with  $\gamma_s = 58.50 \text{ mJ/m}^2$ . The particle clusters form only below the dewetted droplets. Inset d2 shows that the interface at the bare, dewetted areas of the film is smooth and devoid of any particle clusters.

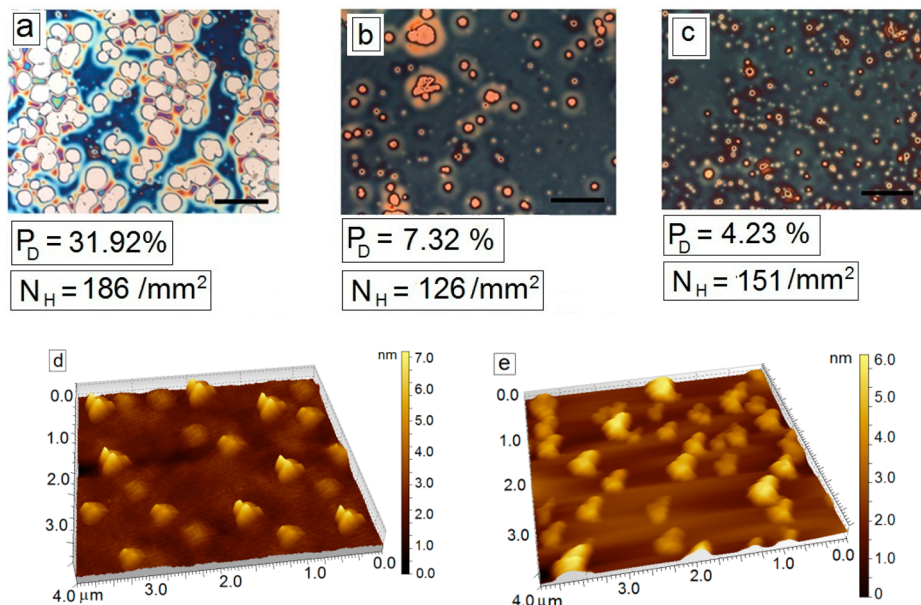


**Figure 6.** (a–c) Optical microscopy images of completely dewetted 112 nm thick films with  $C_{NP} = 0.625\%$  on substrates with  $\gamma_S$  = (a) 28.04, (b) 42.31, and (c) 58.50 mJ/m<sup>2</sup>. Scale bar  $n$  all the frames = 100  $\mu$ m. The percentage of dewetting ( $P_D$ ) and the number density of holes ( $N_H$ ) are marked in each frame. (d, e) Isolated particle clusters seen on substrates with  $\gamma_S$  = 46.53 and 58.50 mJ/m<sup>2</sup>, respectively, after peeling of the dewetted film.

everywhere, including areas of the film exposed during dewetting as well as areas buried under the dewetted droplets. Similar featureless interface is observed in all the dewetted films with  $C_{NP} = 0.1\%$  and  $0.2\%$  on all substrates as long as  $\gamma_S \leq 42.31$  mJ/m<sup>2</sup>. This confirms that in regime 1A (low  $C_{NP}$  films on low  $\gamma_S$  substrates) no particle migrates to the film–substrate interface during thermal annealing and dewetting. In contrast, Figure 5d shows an enriched particle layer, after dewetting of a film with  $C_{NP} = 0.1\%$  on a substrate with  $\gamma_S = 58.5$  mJ/m<sup>2</sup>. AFM scans at different locations of the dewetted film further reveals that the enriched layer is present only below the dewetted droplets (inset d2, Figure 5d) and not over the areas where the film has ruptured and dewetted. Formation of similar interfacial particle clusters only below the dewetted droplets is observed in all films with  $C_{NP} = 0.1\%$  and  $0.2\%$  on substrates with  $\gamma_S \geq 46.53$  mJ/m<sup>2</sup>. It has already been checked in the context of Figure 2 that the interface was featureless right after spin coating for this  $C_{NP}$ – $\gamma_S$  combination and therefore it can be unequivocally argued that the NPs migrate to the substrate–film interface and form isolated particle clusters in regime 1B during thermal annealing and dewetting. Image analysis reveals that the fractional coverage of the substrate by the dewetted droplets varies between 8.96% and 10.03% for films having  $C_{NP} = 0.1\%$  and between 7.34% and 10.21% for films having  $C_{NP} = 0.2\%$ , which is nearly constant within error bar.

At this point we recall that migration of particles to the film–substrate interface during thermal annealing of a polymer film is a complex process involving potential competitive adsorption kinetics rates and release of long-chain polymer molecules which get attached to the substrate during film coating.<sup>43,58,59</sup> The conformational entropy of a polymer molecule increases when a fraction of the particle present in the film matrix migrates to the film–substrate interface.<sup>60</sup> Further, as the particles get adsorbed on the substrate, they release the initially attached long-chain polymer molecules from there, which in turn further enhances their conformational entropy.<sup>45</sup> In simple terms, in order to gain conformational entropy, the polymer molecules induce an effective attraction between the substrate

and the particles, which is known as depletion attraction.<sup>60</sup> Also, the gain in the conformational entropy of the polymer chains upon detachment from the substrate is proportional to the volume of the nanoparticles present in the system.<sup>43</sup> In light of the above considerations, our findings reveal that particle migration in low  $C_{NP}$  films is suppressed on low  $\gamma_S$  substrates ( $\gamma_S \leq 43$  mJ/m<sup>2</sup>) as long as  $\gamma_S \leq \gamma_{C60}$ . We argue that as the gain in the conformational entropy upon detachment of the polymer chains from the substrate is proportional to  $C_{NP}$ , the total gain of energy is low in a low  $C_{NP}$  film, and therefore particle migration is not favored entropically, irrespective of  $\gamma_S$ . Additionally, both  $E_p$  and  $\Delta G_{C60-PS-S}$  are also low on low  $\gamma_S$  substrates, though they become significantly higher, and therefore particle migration becomes favored from the standpoint of interfacial (enthalpic) interactions with gradual increase in  $\gamma_S$ , which substantiates our observation of particle cluster formation on higher  $\gamma_S$  substrates.

In regime 1A as the particles remain within the film matrix on low  $\gamma_S$  substrates, their presence potentially alters the rheological properties and retards the dewetting dynamics in comparison to a particle free film on an identical  $\gamma_S$  substrate.<sup>30,40</sup> A slower dewetting dynamics allows more number of holes to nucleate in the intact parts of the film, resulting in higher values of  $N_N$  in a particle containing film in regime 1A, as compared to a particle free film. The dynamics of the film becomes slower with increase in  $C_{NP}$ , and consequently  $N_N$  is seen to increase with increase in  $C_{NP}$  in this regime. On the other hand, in regime 1B despite migration of the particles to the interface, dewetting still does not get suppressed. This along with the observations that the enriched particle clusters form only below the dewetted droplets and  $N_N$  is nearly independent of  $C_{NP}$  (Figure 4) allows us to indirectly conclude about the relative time scales of particle migration and dewetting in this regime. We argue that the particles migrate to the interface and form clusters at a much faster rate, even before the film has ruptured. However, as  $C_{NP}$  is low, the particle layer fail to cover the entire substrate. The vertical scale bar in Figure 5d is around 7 nm, which emphasizes that the

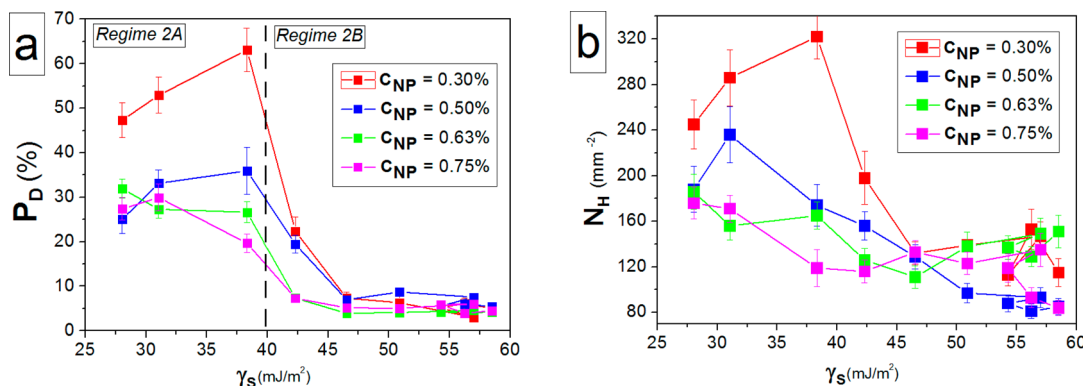


**Figure 7.** Variation of (a) percentage dewetted area ( $P_D$ ) and (b) number density of holes ( $N_H$ ) as a function of substrate surface energy ( $\gamma_s$ ) for films with  $C_{NP}$  in the range of 0.3% and 0.75%.

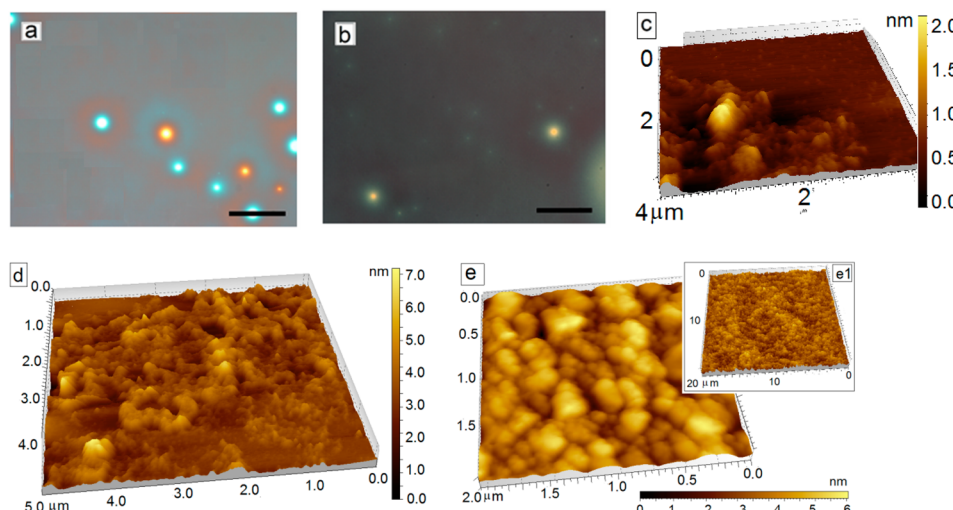


**Figure 8.** Optical microscopy images of 112 nm thick films with  $C_{NP} = 1.0\%$ , annealed for 46 h at 130 °C, with no sign of dewetting on substrates with (a)  $\gamma_s = 28.04 \text{ mJ/m}^2$  and (b)  $\gamma_s = 58.50 \text{ mJ/m}^2$ . (c) Typical AFM morphology of the tiny clusters formed on the film surface. (d, e) Morphology of the substrate–film interface after peeling the film on low ( $\gamma_s = 31.05 \text{ mJ/m}^2$ ) and high surface energy ( $\gamma_s = 58.50 \text{ mJ/m}^2$ ) substrates, respectively. Inset e1 shows that the particle clusters on a high  $\gamma_s$  substrate is very uniform and spans over a large area. The vertical scale bar in (e) is valid for the main figure as well as the inset.

particle cluster is 2–3 particle layers thick. After migration of the particles and formation of the interfacial clusters, there exists an intermediate stage where we have a continuous PS film on an effectively heterogeneous substrate. Following the logic by Barnes et al., the film is completely stable over the  $C_{60}$  clusters<sup>1</sup> and therefore ruptures over the zones of the substrate which are not covered by the interfacial particle layer. It is known that a film on a chemically heterogeneous substrate ruptures due to the in-plane wettability gradient between the distinct surface energy zones (in this case, bare substrate and the NP clusters), and the number density of the nucleated holes depend on the number density of the heterogeneous patches. The fractional particle coverage of a substrate on the other hand is a function of the volume fraction of NPs present in the system and depends only on  $C_{NP}$ . As a result,  $N_N$  becomes independent of  $\gamma_s$  for a specific  $C_{NP}$  irrespective of  $\gamma_s$ . This conclusion is further substantiated by the observation that  $N_N$  actually reduces with increase of  $C_{NP}$  from 0.1% to 0.2%. With increase of  $C_{NP}$ , the number density of the interfacial clusters, which act as differential wettability patches, increases. This in turn results in rupture of the film at larger number of locations, resulting in higher number of nucleated holes. As a consequence, the value of  $N_N$  reduces on a substrate with

same  $\gamma_s$  when  $C_{NP}$  increases. The holes grow over the bare zones of the substrate and the dewetted polymer accumulates over the interfacial clusters, fully covering them, which has been captured clearly in Figure 5d.

**Partial Dewetting of Films with Intermediate NP Concentration (0.3% <  $C_{NP}$  < 0.75%).** The three frames of Figure 6 show the dewetted morphology of a film with  $C_{NP} = 0.625\%$  on substrates with  $\gamma_s = 28.04, 42.31$ , and  $58.50 \text{ mJ/m}^2$ , respectively. The dewetted morphology of the films on other  $\gamma_s$  substrates for  $C_{NP} = 0.3\%, 0.5\%, 0.625\%$ , and  $0.75\%$  are shown in Figures S8–S11 of the Supporting Information, and the corresponding percentage of dewetting ( $P_D$ ) and the number density of holes ( $N_H$ ) are marked in each frame. From these figures, it can be seen that the films dewet up to the level of hole growth and partial coalescence as long as  $\gamma_s \leq 43 \text{ mJ/m}^2$  (regime 2A). In contrast, smaller isolated holes with no sign of coalescence is observed when  $\gamma_s \geq 43 \text{ mJ/m}^2$  (regime 2B). The variation of  $P_D$  and  $N_H$  as a function of  $\gamma_s$  is shown in Figures 7a and 7b, respectively.

It can be seen that in regime 2B  $P_D$  drops precipitously to below 5% and becomes independent of  $\gamma_s$ . We have already argued that particle migration to the interface become favored when  $\gamma_s \geq \gamma_{C60}$ , as  $E_p$  enhances significantly in this range,

indicating preferential migration of the particles. We feel that the sudden transition in the nature of variation of  $P_D$  can be attributed to particle migration and formation of interfacial particle clusters. As  $C_{NP}$  is higher in regime 2B, in comparison to regime 1B, the number density of the particle clusters is higher, which in turn pins the contact line more effectively, prevents hole coalescence, and consequently arrests dewetting at an early stage. This can be confirmed from Figures 6d and 6e, which show the NP clusters at the film–substrate interface after annealing a film with  $C_{NP} = 0.625\%$  on substrates having  $\gamma_S = 46.53$  and  $58.50 \text{ mJ/m}^2$ , respectively. The number density of particle clusters is roughly same in the two figures ( $N_C = 1.22/\mu\text{m}^2$  in Figure 6d and  $1.18/\mu\text{m}^2$  in Figure 6e), which confirms the conjecture that the fractional coverage of the substrate by the particle clusters is nearly independent of  $\gamma_S$ . On the other hand, the film–substrate interface is devoid of any particle clusters on low  $\gamma_S$  substrates for films with  $C_{NP}$  in this range, which can be seen in Figure S12 of the Supporting Information. This implies that, similar to regime 1A, in regime 2A as well particles do not migrate to the interface, as long as  $\gamma_S \leq \gamma_{C_60}$ . However, dewetting is arrested at an intermediate stage due to the partial stabilization is brought about by rheological modification of the polymer in the presence of the particles which is stronger than regime 1A due to higher concentration of the particles.<sup>30</sup> Enhanced viscosity brought about by the presence of particles also makes the dynamics of dewetting sluggish and allows more number of holes to nucleate in film as  $C_{NP}$  increases, following the same logic as regime 1A, which clearly justifies  $N_H$  for  $C_{NP} = 0.5\%$  to be higher than  $N_H$  for  $C_{NP} = 0.3\%$ . However, Figure 7A shows that this trend gets altered when  $C_{NP}$  exceeds 0.5%. We argue that the enhanced viscosity at higher  $C_{NP}$  imparts additional resistance to the growth of the thermally excited surface fluctuations on the free surface of the film, which in turn screens hole formation thereby reducing the number density of holes once  $C_{NP}$  exceeds 0.5%.

**Complete Suppression of Dewetting of Films with High NP Concentration ( $C_{NP} > 1.0\%$ ).** For films with  $C_{NP} \geq 1.0\%$ , complete suppression of dewetting is observed irrespective of  $\gamma_S$  on the time scales of our experiments. Figures 8a and 8b show an intact film with  $C_{NP} = 1.0\%$  on substrates having  $\gamma_S = 28.04$  and  $58.50 \text{ mJ/m}^2$ , respectively, after 46 h of thermal annealing. The observation is commensurate with earlier results by Barnes et al.<sup>1</sup> and subsequently by many others.<sup>21–28,31–39</sup> As observable, however, some clustering of nanoparticles commonly occurs during the film stabilization process. This is not surprising given that our estimate shows the PS– $C_{60}$  interaction is mildly unfavorable,  $\gamma_{C_60-PS} \approx 5.08 \text{ mJ/m}^2$ . Figures 8d and 8e show the formation of a rather uniform layer of particle clusters on substrates having  $\gamma_S = 31.05$  and  $58.50 \text{ mJ/m}^2$ , respectively. Similar diffuse particle layer is seen to form on all substrates, irrespective of  $\gamma_S$  when  $C_{NP} \geq 1.0\%$ . It may be recalled that Figure 2 shows particle migrating to the film–substrate interface during spin coating itself, irrespective of the  $\gamma_S$  of the substrate, which highlights a possible depletion attraction type mechanism active during spin coating itself (without any thermal annealing) for films with relatively higher  $C_{NP}$ . To the best of our knowledge, this is an exciting new observation and needs to be explored in greater details. Comparison of Figures 8d,e with Figures 2a,b allows us to very clearly conclude that during thermal annealing, larger numbers of NPs migrate to the interface and form a diffused particle rich layer. Both Figures 2a and 8d clearly show that the particles migrate to the interface

even when  $\gamma_S \leq \gamma_{C_60}$ , a condition under which particle migration to the interface remains suppressed for low and intermediate  $C_{NP}$  films due to unfavorable surface energy effects. However, as the gain in conformational entropy upon detachment of the polymer molecules from the substrate is proportional to  $C_{NP}$ , therefore we feel that the total gain in entropy offsets the unfavorable enthalpic interaction and forces the particles to migrate to the interface.

**Qualitative Understanding Based on Cahn–Hilliard Model.** We have estimated the  $\chi_{PS-C_{60}}$  values at annealing temperatures of  $130^\circ\text{C}$  based on literature values of  $\delta_{PS}$  and  $\delta_{C_{60}}$  and observe that  $\chi_{PS-C_{60}}$  lies between 0.17 and 0.63 (refer to Supporting Information). For PS with molecular weight 3K, this translates to  $\chi_N > 2$ , which is the necessary condition for blend phase separation. This suggests that PS and  $C_{60}$  phase separate at elevated temperatures. Indeed, we have seen large clusters of  $C_{60}$  in PS films previously and here at sufficiently high  $C_{NP}$ .

Under these phase-separated conditions, at boundaries, if the  $C_{60}$  was the wettable component, we should have observed surface directed spinodal decomposition waves predicted from the Cahn–Hilliard model, rather than exponentially decaying surface segregation as modeled by Binder et al. which would have occurred in the single phase region.<sup>62</sup> We argue that in our system this wettable regime occurs only when  $\gamma_S \geq 43 \text{ mJ/m}^2$ . While we observe the  $C_{60}$  surface transition above  $43 \text{ mJ/m}^2$ , we did not perform neutron reflection (NR) to see if these waves exist, as their wavelength for the nanoparticle scale would be too small to detect even with NR anyway. Assuming there is no shift of phase boundary in these thin films, in the nonwetting region of  $\gamma_S \leq 43 \text{ mJ/m}^2$ , we do not expect any wetting layer, but given near wetting interaction conditions in the proximity to a phase-separated system, a thin prewetting layer may exist, whose decay length should increase as we approach wetting conditions of  $43 \text{ mJ/m}^2$ . Again, NR would be required to verify this prewetting layer and its growth close to wetting conditions. Potentially, we will do this study in future experiments. This layer does not exist at the air boundary as we are too far from  $C_{60}$  wetting conditions. Essentially, we have considered the alternate explanation of surface induced depletion attraction layer in this regard.

## CONCLUSION

In conclusion, we have shown that substrate surface energy ( $\gamma_S$ ) plays an important role in suppression of dewetting of thin polymer films containing  $C_{60}$  NP fillers. It was believed that in such a system the particles migrate to the substrate due to entropic interactions and form a immobilized layer of the NP on the substrate, which either arrest the hole growth by pinning (for low  $C_{NP}$ ) or completely suppress dewetting by effectively altering the wettability of the substrate (for high  $C_{NP}$ ).<sup>1</sup> On the basis of systematic investigations of dewetting of 112 nm thick PS films containing different  $C_{NP}$  of fullerene NP on substrates with different  $\gamma_S$ , we have shown that the migration of the particles to the substrate and formation of the immobilized surface layer is strongly nanoparticle surface energy driven only when  $\gamma_S > \gamma_P$ , particularly when  $C_{NP}$  is less than critical  $C_{NP} \approx 1 \text{ wt \%}$ . We believe that much weaker forces involving phase separation and total system interfacial energy minimization drives the nanoparticles to the substrate interface when  $\gamma_S < \gamma_{C_60}$ . Furthermore, the order of the transition and the sensitivity of the individual thermodynamic transitions for  $\gamma_S > \gamma_P$  and  $\gamma_S <$

$\gamma_p$  regimes are smeared out in the high limit of  $C_{NP} \geq 1$  wt % relative to polymer. These transitions become more a continuum phenomena across a broad range of  $\gamma_s$  as the system approaches toward the jamming limit of nanoparticle systems. Clustering and other effects are consequently observed above this concentration limit. From a practical standpoint, this may be of most interest in forming film stabilizing conductive interfacial layers and is likely to find application in fabrication of polymer fullerene solar cells.<sup>60</sup>

As a final summary, we have presented experimental evidence that tend to suggest the existence of prewetting below  $\gamma_s$  of 43 mJ/m<sup>2</sup>, which is an alternative argument to depletion attraction that explains the influence of  $\gamma_s$  on migration of particles to the film–substrate interface during annealing. We also note that for higher  $C_{NP}$  particle migration to the interface may actually start during film coating itself, even before any thermal annealing. These observations needs to be investigated in greater details to gain further insight into the complex dynamics of NPs within polymer matrix and films.

## ■ ASSOCIATED CONTENT

### ● Supporting Information

Figures S1–S14 and Tables S1, S2. This material is available free of charge via the Internet at <http://pubs.acs.org>.

## ■ AUTHOR INFORMATION

### Corresponding Authors

\*(A.K.) Tel +1-330-972-8324, e-mail alamgir@uakron.edu.

\*(R.M.) Tel +91-3222-283912, e-mail rabibrata@che.iitkgp.ernet.in.

### Notes

The authors declare no competing financial interest.

## ■ ACKNOWLEDGMENTS

The authors thank IUSSTF–Indo US Centre for Research Excellence on Fabrionics for funding the work in the form of faculty and student visits between IIT Kharagpur and University of Akron. This work was supported at the University of Akron by the U.S. Department of Energy (DOE-BES Grant DE-FG02-10ER4779), and the work was performed at the Akron Functional Materials Center (AFMC) funded by the Austen BioInnovation Institute in Akron (ABIA). A.K. also acknowledges the support of ACS-PRF grant for partial support of the work. R.M. acknowledges the Department of Science & Technology (DST), New Delhi, India, for funding the portion of the work carried out at IIT Kharagpur under its Solar Energy Research Initiative program (Grant DST/TM/SERI/2K10/22).

## ■ REFERENCES

- Barnes, K. A.; Karim, A.; Douglas, J. F.; Nakatani, A. I.; Gruell, H.; Amis, E. J. *Macromolecules* **2000**, *33*, 4177–4185.
- Roy, S.; Ansari, K. J.; Jampa, S. S. K.; Vutukuri, P.; Mukherjee, R. *ACS Appl. Mater. Interfaces* **2012**, *4*, 1887–1896.
- Xie, R.; Karim, A.; Douglas, J. F.; Han, C. C.; Weiss, R. A. *Phys. Rev. Lett.* **1998**, *81*, 1251–1254.
- Sharma, A.; Mittal, J. *Phys. Rev. Lett.* **2002**, *89*, 186101.
- Reiter, G.; Hamieh, M.; Damman, P.; Sclavons, S.; Gabriele, S.; Vilmin, T.; Raphaël, E. *Nat. Mater.* **2005**, *4*, 754–758.
- Seemann, R.; Herminghaus, S.; Jacobs, K. *Phys. Rev. Lett.* **2001**, *86*, 5534–5537.
- Reiter, G. *Phys. Rev. Lett.* **1992**, *68*, 75–78.
- Sharma, A.; Reiter, G. *J. Colloid Interface Sci.* **1996**, *178*, 383–399.
- Sharma, A. *Eur. Phys. J. E* **2003**, *12*, 397–408.
- Bäumchen, O.; Jacobs, K. *J. Phys.: Condens. Matter* **2010**, *22*, 033102.
- Xue, L.; Han, Y. *Prog. Polym. Sci.* **2011**, *36*, 269–293.
- Kargupta, K.; Sharma, A. *Phys. Rev. Lett.* **2001**, *86*, 4536–4539.
- Sehgal, A.; Ferreiro, V.; Douglas, J. F.; Amis, E. J.; Karim, A. *Langmuir* **2002**, *18*, 7041–7048.
- Bhandaru, N.; Das, A.; Salunke, N.; Mukherjee, R. *Nano Lett.* **2014**, *14*, 7009–7016.
- Gentili, D.; Foschi, G.; Valle, F.; Cavallini, M.; Biscarini, F. *Chem. Soc. Rev.* **2012**, *41*, 4430–4443.
- Yerushalmi-Rozen, R.; Klein, J.; Fetters, L. J. *Science* **1994**, *263*, 793–795.
- Kerle, T.; Yerushalmi-Rozen, R.; Klein, J.; Fetters, L. J. *Europhys. Lett.* **1998**, *44*, 484–490.
- Carroll, G. T.; Sojka, M. E.; Lei, X.; Turro, N. J.; Koberstein, J. *Langmuir* **2006**, *22*, 7748–7754.
- Henn, G.; Bucknall, D. G.; Stamm, M.; Vanhoorne, P.; Jerome, R. *Macromolecules* **1996**, *29*, 4305–4313.
- Feng, Y.; Karim, A.; Weiss, R. A.; Douglas, J. F.; Han, C. C. *Macromolecules* **1998**, *31*, 484–493.
- Barnes, K. A.; Douglas, J. F.; Liu, D.-W.; Karim, A. *Adv. Colloid Interface Sci.* **2001**, *94*, 83–104.
- Holmes, M. A.; Mackay, M. E.; Giunt, R. K. *J. Nanopart. Res.* **2007**, *9*, 753–763.
- Han, J. T.; Lee, G. W.; Kim, S.; Lee, H. J.; Douglas, J. F.; Karim, A. *Nanotechnology* **2009**, *20*, 105705.
- Wong, H. C.; Cabral, J. T. *Phys. Rev. Lett.* **2010**, *105*, 038301.
- Wong, H. C.; Cabral, J. T. *Macromolecules* **2011**, *44*, 4530–4537.
- Sharma, S.; Rafailovich, M. H.; Peiffer, D.; Sokolov, J. *Nano Lett.* **2001**, *1*, 511–514.
- Krishnan, R. S.; Mackay, M. E.; Duxbury, P. M.; Hawker, C. J.; Asokan, S.; Wong, M. S.; Goyette, R.; Thiagarajan, P. *J. Phys.: Condens. Matter* **2007**, *19*, 356003.
- Kanemoto, R.; Anas, A.; Matsumoto, Y.; Ueji, R.; Itoh, T.; Baba, Y.; Nakanishi, S.; Ishikawa, M.; Biju, V. *J. Phys. Chem. C* **2008**, *112*, 8184–8191.
- Xavier, J. H.; Sharma, S.; Seo, Y. S.; Isseroff, R.; Koga, T.; White, H.; Ulman, A.; Shin, K.; Satija, S. K.; Sokolov, J.; Rafailovich, M. H. *Macromolecules* **2006**, *39*, 2972–2980.
- Mukherjee, R.; Das, S.; Das, A.; Sharma, S. K.; Raychaudhuri, A. K.; Sharma, A. *ACS Nano* **2010**, *4*, 3709–3724.
- Krishnan, R. S.; Mackay, M. E.; Hawker, C. J.; Van Horn, B. *Langmuir* **2005**, *21*, 5770–5776.
- Mackay, M. E.; Hong, Y.; Jeong, M.; Hong, S.; Russell, T. P.; Hawker, C. J.; Vestberg, R.; Douglas, J. F. *Langmuir* **2002**, *18*, 1877–1882.
- Hosaka, N.; Tanaka, K.; Otsuka, H.; Otsuka, H.; Takahara, A. *Compos. Interfaces* **2004**, *11*, 297–306.
- Hosaka, N.; Tanaka, K.; Otsuka, H.; Otsuka, H.; Takahara, A. *Langmuir* **2007**, *23*, 902–907.
- Hosaka, N.; Otsuka, H.; Hino, M.; Takahara, A. *Langmuir* **2008**, *24*, 5766–5772.
- Wei, B.; Gurr, P. A.; Genzer, J.; Qiao, G. G.; Solomon, D. H.; Spontak, R. J. *Macromolecules* **2004**, *37*, 7857–7860.
- Kropka, J. M.; Green, P. F. *Macromolecules* **2006**, *39*, 8758–8762.
- Xue, L.; Cheng, Z.; Fu, J.; Han, Y. *J. Chem. Phys.* **2008**, *129*, 054905.
- Xu, L.; Yu, X.; Shi, T.; An, L. *Soft Matter* **2009**, *5*, 2109.
- Besancon, B. M.; Green, P. F. *Macromolecules* **2005**, *38*, 110–115.
- Koo, J.; Shin, K.; Seo, Y.-S.; Koga, T.; Park, S.; Satija, S.; Chen, X.; Yoon, K.; Hsiao, B. S.; Sokolov, J. C. *Macromolecules* **2007**, *40*, 9510–9516.
- Lee, J. Y.; Buxton, G. A.; Balazs, A. C. *J. Chem. Phys.* **2004**, *121*, 5531–5539.

- (43) Krishnamoorti, R.; Vaia, R. A. *J. Polym. Sci., Part B: Polym. Phys.* **2007**, *45*, 3252–3256.
- (44) Kropka, J. M.; Putz, K. W.; Pryamitsyn, V.; Ganesan, V.; Green, P. F. *Macromolecules* **2007**, *40*, 5424–5432.
- (45) Krishnan, R. S.; Mackay, M. E.; Duxbury, P. M.; Pastor, A.; Hawker, C. J.; Horn, B. V.; Asokan, S.; Wong, M. S. *Nano Lett.* **2007**, *7*, 484–489.
- (46) McGarry, E. S.; Duxbury, P. M.; Mackay, M. E.; Frischknecht, A. L. *Macromolecules* **2008**, *41*, 5952–5954.
- (47) Wong, H. C.; Higgins, A. M.; Wildes, A. R.; Douglas, J. F.; Cabral, J. T. *Adv. Mater.* **2013**, *25*, 985–991.
- (48) Chen, X. C.; Green, P. F. *Soft Matter* **2011**, *7*, 1192–1198.
- (49) Maillard, D.; Kumar, S. K.; Rungta, A.; Benicewicz, B. C. *Nano Lett.* **2011**, *11*, 4569–4573.
- (50) Chandran, S.; Begum, N.; Padmanabhan, V.; Basu, J. K. *Nat. Commun.* **2014**, *5*, 3697.
- (51) Bandyopadhyay, D.; Douglas, J. F.; Karim, A. *Macromolecules* **2011**, *44*, 8136–8142.
- (52) Bandyopadhyay, D.; Douglas, J. F.; Karim, A. *Macromolecules* **2012**, *45*, 4716–4722.
- (53) Smith, A. P.; Sehgal, A.; Douglas, J. F.; Karim, A.; Amis, E. J. *Macromol. Rapid Commun.* **2003**, *24*, 131–135.
- (54) Mukherjee, R.; Sharma, A. *ACS Appl. Mater. Interfaces* **2012**, *4*, 355–362.
- (55) Ma, X.; Wigington, B.; Bouchard, D. *Langmuir* **2010**, *26*, 11886–11893.
- (56) Kargupta, K.; Sharma, A. *Langmuir* **2002**, *18*, 1893–1903.
- (57) Muller-Buschbaum, P.; Bauer, E.; Wunnicke, O.; Stamm, M. J. *Phys.: Condens. Matter* **2005**, *17*, S363–S386.
- (58) Gupta, S.; Zhang, Q.; Emrick, T.; Balazs, A. C.; Russell, T. P. *Nat. Mater.* **2006**, *5*, 229–233.
- (59) Luo, H.; Gersappe, D. *Macromolecules* **2004**, *37*, 5792–5799.
- (60) Lee, J. Y.; Shou, Z.; Balazs, A. C. *Phys. Rev. Lett.* **2003**, *91*, 136103.
- (61) Wong, H. C.; Li, Z.; Tan, C. H.; Zhong, H.; Huang, Z.; Bronstein, H.; McCulloch, I.; Cabral, J. T.; Durrant, J. R. *ACS Nano* **2014**, *8*, 1297–1307.
- (62) Muller, M.; Albano, E. V.; Binder, K. *Phys. Rev. E* **2000**, *62*, 5281–5295.